



Cite this: DOI: 10.1039/c7nj04932c

A comparison of optical, electrochemical and self-assembling properties of two structural isomers based on 1,6- and 1,8-pyrenedione chromophores†

Samantha N. Keller and Todd C. Sutherland *

Two isomeric donor–acceptor–donor (DAD) pyrene chromophores were synthesized and their optical, electrochemical and solid-state properties were investigated. Both chromophores showed similar light absorption profiles that spanned the visible region from 300 nm to 800 nm, in part due to strong intramolecular charge transfer bands. Both 1,6- and 1,8-pyrenediketone acceptor cores exhibited similar reversible electrochemical reductions at potentials of -0.91 V and -0.86 V *versus* ferrocene/ferrocenium, respectively, which yields approximate LUMO energy levels of -3.9 eV *versus* vacuum. By design, both DAD chromophores displayed both electro- and halochromism. Despite their similar structure, only the 1,6-pyrenediketone derivative exhibited self-assembly in the solid-state by forming a soft crystalline phase. Furthermore, the solid-state film absorption profile of the 1,6-pyrenediketone isomer showed a significant change in the absorption profile upon annealing above its cold-crystallisation temperature, providing an absorption band that extends to 900 nm, suggesting strong intermolecular electronic interactions.

Received 12th December 2017,
Accepted 19th January 2018

DOI: 10.1039/c7nj04932c

rsc.li/njc

Introduction

The polycyclic aromatic hydrocarbon pyrene, has been of interest to the synthetic organic^{1–3} and photochemistry^{4–6} communities for a long time, as evidenced by extensive review articles. To the synthetic community, pyrene is a challenging substrate to poly-functionalise in a chemo- and regio-selective manner, whereas, the photochemistry community is interested in developing models that pertain to the excimer formation dynamics and their potential applications. Because of the fundamental research conducted on pyrene, there is an extensive list of applications that have been built on this core in areas such as photocatalysts,⁷ organic semiconductors,^{8,9} bio-sensing/imaging,^{10,11} liquid crystals,^{8,12–16} covalent organic frameworks,^{17,18} and organogelators.^{13,19}

Despite pyrene's photophysical prominence, it is a relatively poor chromophore in the visible region of the spectrum. Unsubstituted pyrene has electronic absorption peaks between 220 nm and 350 nm and molar absorption coefficients of approximately $50\,000\text{ M}^{-1}\text{ cm}^{-1}$ in cyclohexane. Two approaches are generally taken to enhance the chromophore's intensity and

absorption profile: (1) extending pi-conjugation and (2) donor–acceptor. Several examples of pyrenes containing either vinylic^{20–23} or acetylenic^{23,24} linkages to other pi-systems have shown a general red-shift in the absorption spectra, dependent on the attachment location. Likewise, the donor–acceptor approach has generated several example pyrene-based chromophores with lower energy absorption peaks than pyrene.^{24–29} Due to pyrene's energetically accessible frontier molecular orbitals, it has been exploited as either an electron donor^{30,31} or an acceptor.^{32–36}

In addition to improving the light absorption properties, there is interest in designing materials that self-assemble, which has been proposed as a method to enhancing charge transport in the solid-state.^{37–40} The notion that self-assembling pi-systems will enhance the overlap of intermolecular frontier molecular orbitals such that efficient charge migration could occur. Our goal is twofold. First, to increase the light absorption properties of pyrene using both pi-extension and donor–acceptor strategies. Second, to add self-assembling functionality to the pyrene chromophore by including structural features proposed to impart liquid crystalline properties based on previous reports^{8,12–16} of pyrene derivatives.

In our previous contributions,^{27,41} we explored the regio-isomeric and structure–property relationships of different donor positions on various pyrene acceptor chromophores, as shown in Chart 1. Previously, the pyrene scaffold was altered to have

Department of Chemistry, University of Calgary, 2500 University Drive NW, Calgary, Alberta, T3G 1M1, Canada. E-mail: todd.sutherland@ucalgary.ca

† Electronic supplementary information (ESI) available. See DOI: 10.1039/c7nj04932c

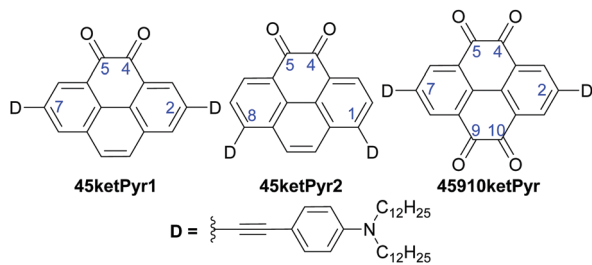


Chart 1 Summary of our previous DAD chromophores based on pyrene ketones.

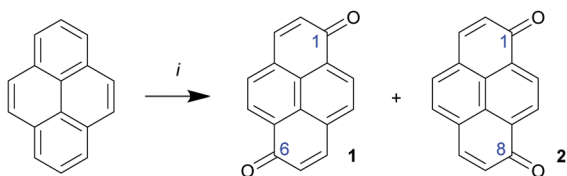
both donors (D) and acceptors (A) arranged as DAD chromophores, whereby the acceptor functionality was based on *ortho*-diketone derivatives of pyrene and the donors were based on 4-alkynylaniline derivatives. Here we present two structural isomers of pyrene diketones, 1,6- and 1,8-pyrene diketones, which are produced as a mixture upon oxidation of pyrene with chromic acid, as shown in Scheme 1.⁴² There are few reports of pyrene-based organic materials with this substitution pattern. None of our previous pyrene *ortho*-diketones exhibited self-assembling solid-state properties, however, there is literature precedence for liquid crystalline behaviour of compounds based on pyrene-1,6 and 1,8-diketones.⁸ Hirose and co-workers⁸ reported a series of 1,6- and 1,8-diketones that featured alkoxy substituents with varying alkyl chain lengths that displayed discotic lamellar mesophases with absorption properties spanning to approximately 525 nm. Our motivation is threefold to understand the regioisomeric effects of D–A positions on a pyrene scaffold. (1) To generate strong chromophores; (2) access low energy reduction potentials; (3) probe solid-state organization of soft materials. Using ketones as acceptor motifs, others^{43–45} have demonstrated assembly of fluorenone derivatives into microfibers with enhanced nonlinear optical properties. The pyrene DAD architectures may lead to large two-photon absorption cross sections, which are of interest to the photonics community.

Here we present the synthesis, optical, electrochemical and self-assembling properties of 1,6- and 1,8-pyrenediketones that are appended to pi-conjugated 4-ethynylanilines donors, yielding DAD chromophores. Moreover, the chromophores have broad absorption profiles to 800 nm and show soft crystalline features in the solid-state.

Experimental section

1 and 2: pyrene-1,6-diketone and pyrene-1,8-diketone

To a solution of $\text{Na}_2\text{Cr}_2\text{O}_7$ (7.7 g, 26 mmol) in aqueous H_2SO_4 (100 mL, 3 M) was added pyrene (5.0 g, 25 mmol), which had



Scheme 1 Chromic acid oxidation of pyrene. (i) $\text{Na}_2\text{Cr}_2\text{O}_7$, H_2SO_4 (3 M), 90 °C, 4 h (mixture of **1** and **2**, 43%).

been crushed to a fine powder prior to addition. The mixture was stirred and heated at 80 °C for 5 h, then poured onto ice and a red solid was collected by filtration. The red product was purified on basic alumina, eluting unreacted pyrene with chloroform, followed by elution of the red product band with ethyl acetate. Removal of the solvent yielded a bright red solid as a mixture of isomers (2.5 g, 11 mmol, 43%). Characterisation data was in agreement with previously reported data for these compounds.⁴⁶ ^1H NMR (300 MHz, chloroform-*d*) δ 8.63 (s, 1H), 8.48 (d, $J = 7.5$ Hz, 1H), 7.83 (d, $J = 7.5$ Hz, 1H), 7.70–7.63 (m, 3H), 6.68 (dd, $J = 9.9, 7.7$ Hz, 2H).

3: 1,6-bis(triisopropylsiloxy)pyrene

To a mixture of pyrene 1,6- and 1,8-diketones **1** and **2** (1.3 g, 5.6 mmol) in dry dichloromethane (100 mL) were added zinc powder (5.5 g, 84 mmol), TMEDA (4.2 mL, 28 mmol) and TIPS-Cl (4.8 mL, 22 mmol). The mixture was stirred at room temperature under a nitrogen atmosphere for 4 h. The zinc was removed by filtration through celite, followed by a DCM silica plug, and the solvent was removed to yield an off-white solid. Crystallization in a mixture of DCM and MeOH yielded the 1,6-bis(triisopropylsiloxy)pyrene **3** as a white powder (1.29 g, 2.36 mmol, 42%). HRMS-MALDI (M^+) calcd for $\text{C}_{34}\text{H}_{50}\text{O}_2\text{Si}_2$: 546.3344, found: 546.3362. ^1H NMR (400 MHz, chloroform-*d*) δ 8.27 (d, $J = 9.1$ Hz, 2H), 7.95 (d, $J = 8.4$ Hz, 2H), 7.92 (d, $J = 9.2$ Hz, 2H), 7.49 (d, $J = 8.2$ Hz, 2H), 1.55–1.42 (m, 6H), 1.25–1.14 (m, 36H). ^{13}C NMR (101 MHz, chloroform-*d*) δ 150.1, 126.7, 126.3, 126.3, 124.6, 122.8, 119.7, 116.5, 18.3, 13.4.

4: 1,8-bis(triisopropylsiloxy)pyrene

In order to isolate the 1,8-bis(triisopropylsiloxy)pyrene, **4**, the solvent was removed from the mother liquor to yield a brown solid, which was further purified on a silica gel plug eluting with DCM. Removal of the solvent afforded a yellow oil that slowly solidified. (1.3 g, 2.3 mmol, 41%) HRMS-MALDI (M^+) calcd for $\text{C}_{34}\text{H}_{50}\text{O}_2\text{Si}_2$: 546.3344, found: 546.3319. ^1H NMR (400 MHz, chloroform-*d*) δ 8.41 (s, 2H), 7.94 (d, $J = 8.3$ Hz, 2H), 7.80 (s, 2H), 7.50 (d, $J = 8.3$ Hz, 2H), 1.56–1.45 (m, 6H), 1.25–1.20 (m, 36H). ^{13}C NMR (101 MHz, chloroform-*d*) δ 150.0, 126.7, 126.1, 125.0, 124.7, 123.0, 121.0, 116.2, 18.3, 13.4.

5: 1,6-dibromo-3,8-bis(triisopropylsiloxy)pyrene

To a solution of 1,6-bis(triisopropylsiloxy)pyrene **3** (0.40 g, 0.73 mmol) in DCM (50 mL) a solution of bromine (0.27 g, 1.7 mmol) in DCM (10 mL) was added dropwise. The mixture was allowed to stir at room temperature for 30 minutes, after which time the reaction was quenched with $\text{Na}_2\text{S}_2\text{O}_3$. The organic solution was washed with water, dried with MgSO_4 , and the solvent was removed to yield a brown solid. The crude solid was purified by column chromatography (hexanes: DCM 19:1) yielding a yellow solid (0.28 g, 0.38 mmol, 52%). HRMS-MALDI (M^+) calcd for $\text{C}_{34}\text{H}_{48}\text{Br}_2\text{O}_2\text{Si}_2$: 702.1554; found: 702.1581. ^1H NMR (400 MHz, chloroform-*d*) δ 8.35–8.27 (m, 4H), 7.78 (s, 2H), 1.56–1.41 (m, 6H), 1.21 (d, $J = 7.5$ Hz, 36H). ^{13}C NMR (101 MHz, chloroform-*d*) δ 150.2, 126.8, 125.2, 125.1, 122.7, 121.3, 121.0, 119.4, 18.3, 13.3.

6: 1,8-dibromo-3,6-bis(triisopropylsiloxy)pyrene

To a solution of 1,8-bis(triisopropylsiloxy)pyrene **4** (0.35 g, 0.64 mmol) in DCM (50 mL) a solution of bromine (0.24 g, 1.5 mmol) in DCM (10 mL) was added dropwise. The mixture was allowed to stir at room temperature for 30 minutes, after which time the reaction was quenched with $\text{Na}_2\text{S}_2\text{O}_3$. The organic solution was washed with water, dried with MgSO_4 , and the solvent was removed to yield a brown solid. The crude solid was purified by column chromatography (hexanes:DCM 4:1) yielding a yellow oil (0.27 g, 0.38 mmol, 60%). HRMS-MALDI (M^+) calcd for $\text{C}_{34}\text{H}_{48}\text{Br}_2\text{O}_2\text{Si}_2$: 702.1554; found: 702.1526. ^1H NMR (400 MHz, chloroform-*d*) δ 8.38 (s, 2H), 8.22 (s, 2H), 7.77 (s, 2H), 1.56–1.44 (m, 6H), 1.22 (d, $J = 7.5$ Hz, 36H). ^{13}C NMR (101 MHz, CDCl_3) δ 150.1, 126.6, 125.0, 124.5, 123.0, 120.9, 120.8, 119.1, 18.1, 13.1.

7

1,6-Dibromo-3,8-bis(triisopropylsiloxy)pyrene **5** (0.10 g, 0.14 mmol) was dissolved in dry triethylamine (10 mL) under a nitrogen atmosphere. $\text{PdCl}_2(\text{dppf})$ (0.01 g, 0.01 mmol) and CuI (0.005 g, 0.002 mmol) were added, and the mixture was stirred and heated to 80 °C. A 1.0 M solution of the alkyne in triethylamine (0.31 mL, 0.31 mmol) was added slowly over five minutes, and the mixture was then stirred for an additional four hours. The solvent was removed, and the mixture was then purified by column chromatography (9:1 hexanes:DCM) yielding an orange oil (0.11 g, 0.073 mmol, 52%). HRMS-MALDI (M^+) calcd for $\text{C}_{98}\text{H}_{156}\text{N}_2\text{O}_2\text{Si}_2$ 1449.1700; found 1449.1689. ^1H NMR (400 MHz, chloroform-*d*) δ 8.52 (d, $J = 9.3$ Hz, 2H), 8.33 (d, $J = 9.3$ Hz, 2H), 7.60 (s, 2H), 7.56 (d, $J = 9.0$ Hz, 4H), 6.65 (d, $J = 9.0$ Hz, 4H), 3.31 (t, $J = 7.7$ Hz, 8H), 1.62 (t, $J = 7.1$ Hz, 8H), 1.57–1.43 (m, 6H), 1.37–1.25 (m, 72H), 1.22 (d, $J = 7.5$ Hz, 36H), 0.89 (t, $J = 7.2$ Hz, 12H). ^{13}C NMR (101 MHz, chloroform-*d*) δ 149.7, 148.2, 133.2, 130.0, 127.4, 126.5, 125.2, 123.4, 120.2, 119.2, 118.8, 111.5, 96.6, 86.7, 51.2, 32.1, 29.8, 29.8, 29.8, 29.7, 29.5, 27.4, 27.3, 22.9, 18.4, 14.3, 13.4.

8

1,8-Dibromo-3,6-bis(triisopropylsiloxy)pyrene **6** (0.10 g, 0.14 mmol) was dissolved in dry triethylamine (10 mL) under a nitrogen atmosphere. $\text{PdCl}_2(\text{dppf})$ (0.01 g, 0.01 mmol) and CuI (0.005 g, 0.002 mmol) were added, and the mixture was stirred and heated to 80 °C. A 1.0 M solution of the alkyne in triethylamine (0.31 mL, 0.31 mmol) was added slowly over five minutes, and the mixture was then stirred for an additional four hours. The solvent was removed, and the mixture was then purified by column chromatography (9:1 hexanes:DCM) yielding an orange oil (0.097 g, 0.067 mmol, 48%). HRMS-MALDI (M^+) calcd for $\text{C}_{98}\text{H}_{156}\text{N}_2\text{O}_2\text{Si}_2$ 1449.1700; found 1449.1689. ^1H NMR (400 MHz, chloroform-*d*) δ 8.48 (s, 2H), 8.36 (s, 2H), 7.59 (s, 2H), 7.56 (d, $J = 8.9$ Hz, 4H), 6.65 (d, $J = 9.2$ Hz, 4H), 3.32 (t, $J = 7.7$ Hz, 8H), 1.61 (p, $J = 7.6$ Hz, 8H), 1.58–1.47 (m, 6H), 1.40–1.26 (m, 72H), 1.26–1.20 (m, 36H), 0.89 (d, $J = 7.3$ Hz, 12H). ^{13}C NMR (101 MHz, chloroform-*d*) δ 149.5, 148.2, 133.2, 127.2, 126.5, 124.1, 123.6, 121.2, 119.0, 118.9, 111.5, 109.3, 96.7, 86.9, 51.2, 32.1, 29.8, 29.8, 29.8, 29.7, 29.5, 27.5, 27.3, 22.9, 18.4, 14.3, 13.4.

16ketPyr

Compound **7** (0.04 g, 0.03 mmol) was dissolved in dichloromethane (30 mL) and stirred in an open flask. A 1 M solution of tetrabutylammonium fluoride (0.1 mL, 0.10 mmol) was added, and the yellow solution immediately turned pink. The solution was stirred for 10 minutes, after which time DDQ (0.007 g, 0.03 mmol) was added to the mixture, which turned the solution dark green. The mixture was then extracted with water, dried with MgSO_4 , and the solvent was evaporated to yield a dark green solid. The crude solid was purified on an alumina plug, eluting with toluene to yield an emerald green solid (0.029 g, 0.023 mmol, 86%). HRMS-MALDI (M^+) calcd for $\text{C}_{80}\text{H}_{114}\text{N}_2\text{O}_2$ 1134.8875; found 1134.8823. ^1H NMR (400 MHz, chloroform-*d*) δ 8.54 (d, $J = 7.7$ Hz, 2H), 8.45 (d, $J = 7.7$ Hz, 2H), 7.50 (d, $J = 8.6$ Hz, 4H), 6.90 (s, 2H), 6.63 (d, $J = 8.7$ Hz, 4H), 3.32 (t, $J = 7.8$ Hz, 8H), 1.67–1.55 (m, 8H), 1.39–1.24 (m, 72H), 0.88 (t, $J = 6.5$ Hz, 12H). ^{13}C NMR (101 MHz, CDCl_3) δ 184.5, 149.3, 136.2, 134.1, 133.1, 130.6, 130.5, 130.1, 129.5, 127.3, 111.4, 106.8, 105.9, 84.7, 51.2, 32.1, 29.9, 29.8, 29.8, 29.8, 29.7, 29.5, 27.4, 27.3, 22.9, 14.3.

18ketPyr

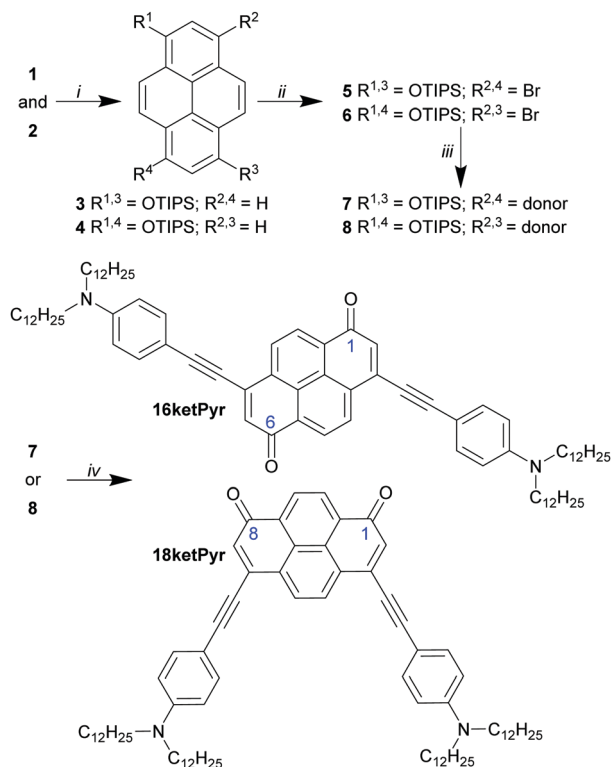
Compound **8** (0.1 g, 0.07 mmol) was dissolved in dichloromethane (30 mL) and stirred in an open flask. A 1 M solution of tetrabutylammonium fluoride (0.2 mL, 0.2 mmol) was added, and the yellow solution immediately turned pink. The solution was stirred for 10 minutes, after which time DDQ (0.02 g, 0.09 mmol) was added to the mixture, which turned the solution dark green. The mixture was then extracted with water, dried with MgSO_4 , and the solvent was evaporated to yield a dark green solid. The crude solid was purified on an alumina plug, eluting with toluene to yield an emerald green solid (0.054 g, 0.048 mmol, 72%). HRMS-MALDI (M^+) calcd for $\text{C}_{80}\text{H}_{114}\text{N}_2\text{O}_2$ 1134.8875; found 1134.8845. ^1H NMR (400 MHz, chloroform-*d*) δ 8.58 (s, 2H), 8.30 (s, 2H), 7.49 (d, $J = 8.8$ Hz, 4H), 6.85 (s, 2H), 6.62 (d, $J = 8.9$ Hz, 4H), 3.32 (t, $J = 8.2$ Hz, 8H), 1.66–1.58 (m, 8H), 1.38–1.25 (m, 72H), 0.89 (t, $J = 6.8$ Hz, 12H). ^{13}C NMR (101 MHz, CDCl_3) δ 184.2, 149.4, 136.4, 134.1, 133.8, 132.5, 130.9, 130.2, 130.0, 129.1, 127.6, 111.5, 107.1, 105.5, 84.7, 51.2, 32.1, 29.8, 29.8, 29.7, 29.5, 27.4, 27.3, 22.8, 14.3.

Results and discussion

Synthesis

The synthesis of the DAD chromophores began with the oxidation of pyrene in chromic acid according to a modification of previously reported procedures.^{42,47–49} Pyrene was added to a solution of sodium dichromate in 3 M H_2SO_4 , and was heated to reflux for four hours as shown in Scheme 1. The resulting red-orange precipitate was filtered through basic alumina, yielding a mixture of the pyrene-1,6 and 1,8-diketones, **1** and **2**, in 43% total yield.

The mixture of diketones was identified by each components diagnostic ^1H NMR spectra. The pyrene-1,6-diketone **1**, possessing C_{2h} symmetry, displays four sets of doublets, while the



Scheme 2 Synthesis of chromophores **16ketPyr** and **18ketPyr**. (i) TIPS-Cl, TMEDA, Zn, DCM (**3**, 42%; **4**, 41%); (ii) Br_2 , DCM (**5**, 52%; **6**, 60%); (iii) *N,N*-didodecyl-4-ethynylaniline (donor), $\text{PdCl}_2(\text{dppf})$, CuI, Et_3N , 80 °C (**7**, 52%; **8**, 48%); (iv) TBAF, DDQ, DCM (**16ketPyr**, 86%; **18ketPyr**, 72%).

1,8-diketone **2**, which is C_{2v} symmetric, displays two doublets and two singlets.

The mixture of diketones was not purified at this point and instead was subjected to reduction followed by silylation, as shown in Scheme 2. The two diketones were reduced with zinc in the presence of TMEDA, and the oxygen atoms were protected with triisopropylsilyl (TIPS) groups to produce a mixture of 1,6-bis-(triisopropylsilyloxy)pyrene **3** and 1,8-bis-(triisopropylsilyloxy)pyrene **4** in 83% total yield. At this point, the resulting mixture was separated into single regioisomers by fractional crystallization in a mixture of chloroform and methanol. The ability to obtain the 1,6- and 1,8-isomers as separate species is significant given the difficulty encountered in separating the diketone mixture of **1** and **2** by chromatography. The diketone mixture was also reduced and protected with TBDMS group, analogous to our *ortho*-diketone previous work,⁴¹ but attempts to separate this mixture by either crystallization or chromatography were unsuccessful. Each of the bis-(triisopropylsilyloxy)-pyrenes **3** and **4** can be easily deprotected and re-oxidized to the corresponding parent diketone using the conditions described later. The reduction and protection reactions were carried out to add solubility and ease purification, but also to enable subsequent cross-coupling reactions.

To continue the synthesis of the DAD chromophores, each of the isolated silylated pyrenes **3** and **4** was treated independently and subjected to electrophilic bromination with Br_2 to produce

dibromides **5** and **6** as shown in Scheme 2. The yields obtained in bromination were modest (50–60%), as the TIPS group is more labile than the robust TBDMS silyl ether. Whether Br_2 or NBS was used as a brominating reagent, the synthesis of dibromides **5** and **6** consistently showed a small amount of de-protected and re-oxidized pyrene-diketone as a side product, which was removed by a silica plug.

The regiochemistry of the bromine atoms relative to the triisopropylsilyloxy groups was determined by HMBC-NMR spectroscopic methods; 1D-NMR spectroscopy was insufficient to assign the structure, as several substitution possibilities would have produced the observed patterns. Pyrene is known to undergo electrophilic aromatic substitution reactions primarily at the 1,3,6, and 8 positions⁹ and there is literature precedence showing that *meta* substitution proceeds even on pyrenes substituted with classical *ortho/para* directors at the 1,6- or 1,8-positions.⁵⁰

The HMBC spectrum showed that the proton signal at 7.78 ppm has four interactions including two quaternary carbons and strong interactions with the TIPS and bromine substituted carbons. Therefore, it can be concluded that dibromide **5** contains bromine atoms substituted *meta* to the triisopropylsilyloxy groups.

Subsequently, dibromides **5** and **6** were subjected to Sonogashira cross coupling with the donor, *N,N*-didodecyl-4-ethynylaniline, to produce the bis-alkynes, **7** and **8** in approximately 50% yields.

Finally, bis-alkynes **7** and **8** were desilylated using TBAF to form the corresponding di-oxyanions followed by oxidation. However, unlike our previous reports of *ortho*-diketones where the desilylation using TBAF and exposure to air resulted in oxidation. Here, neither air nor Ag_2O proved useful in converting the orange di-oxyanionic intermediates into the corresponding 1,6- or 1,8-diketones. Several oxidants were screened including H_2O_2 , NaClO , and 2,3-dichloro-5,6-dicyano-1,4-benzoquinone (DDQ). DDQ oxidation produced the best results in the conversion of the fluorescent solution of intermediates to a non-emissive dark green solution, which after silica gel column chromatography purification yielded dark green DAD chromophores **16ketPyr** and **18ketPyr**, as shown in Scheme 2.

Optical and electrochemical properties

Table 1 lists the pertinent optoelectronic values obtained for the 1,6- and 1,8-regioisomeric DAD chromophores and places them in context with analogous previously reported pyrene-based DAD chromophores. Chloroform solutions of the two DAD chromophores based on 1,6- and 1,8-pyrene diketones are shown in the inset of Fig. 1; both compounds are a dark green colour, but the 1,8-diketo isomer, **18ketPyr**, has more of a blue tint than the 1,6-diketo isomer, **16ketPyr**.

The UV/Vis absorption spectra of **16ketPyr** and **18ketPyr** in chloroform solution are shown in Fig. 1. Both of the chromophores display several electronic transitions, enabling their absorbance profiles to span almost the entire range from 250 to 800 nm. The intramolecular charge transfer (ICT) absorbance bands of **16ketPyr** and **18ketPyr** both have onsets of 800 nm, corresponding to a HOMO–LUMO energy gap of 1.6 eV for both of the isomers. However, the λ_{max} of the ICT band of **16ketPyr**

Table 1 Comparison of optical and electronic properties of DAD chromophores **16ketPyr** and **18ketPyr** with closely related pyrene chromophores

| | ϵ^a ($M^{-1} cm^{-1}$) | $\lambda_{max(onset)}^b$ (nm) | E_{opt}^c (eV) | $E_{ox(DPV)}^d$ (V) | $E_{red(DPV)}^d$ |
|----------------------------------|--------------------------------------|----------------------------------|---------------------|------------------------|------------------|
| 45ketPyr1 ⁴¹ | 7400 | 575(780) | 1.6 | 0.33 | -1.04 |
| 45ketPyr2 ⁴¹ | 23 000 | 570(730) | 1.7 | 0.40 | -1.11 |
| 45910ketPyr ²⁷ | 1700 | 630(880) | 1.4 | 0.43 | -0.84, -1.18 |
| 16ketPyr | 25 000 | 627(800) | 1.6 | 0.47 | -0.91, -1.15 |
| 18ketPyr | 52 000 | 617(800) | 1.6 | 0.47 | -0.86 |

^a Molar absorptivity at the peak of the ICT band. ^b Measured in $CHCl_3$ from lowest energy band. ^c Calculated from λ_{onset} . ^d DPV potentials are referenced to an internal Fc/Fc^+ redox probe in CH_2Cl_2 containing 0.05 M $(nBu)_4PF_6$ with a Pt button working electrode, a Ag wire quasi reference electrode and a Pt wire counter electrode at 20 $mV s^{-1}$.

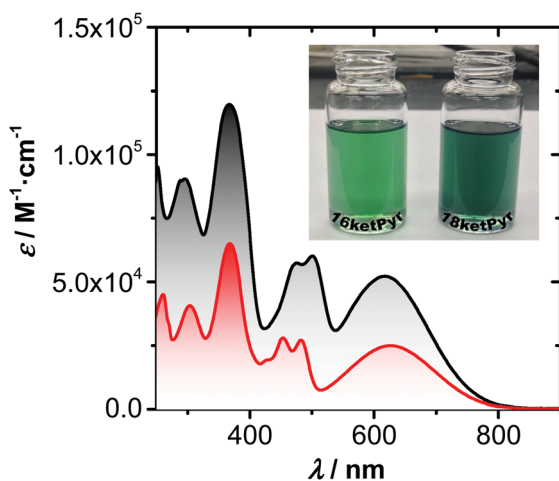


Fig. 1 Absorption of compounds **16ketPyr** (red, left vial) and **18ketPyr** (black, right vial) in $CHCl_3$.

appears at slightly lower energy compared to **18ketPyr** (627 nm vs. 617 nm). Compound **18ketPyr** shows more intense transitions than those of **16ketPyr** at the same concentration (ϵ of the ICT band of **18ketPyr** is 52 000 $M^{-1} cm^{-1}$ compared to 25 000 $M^{-1} cm^{-1}$ for **16ketPyr**), which can be explained in terms of the fact that **18ketPyr** has a greater change in dipole moment upon undergoing electronic transitions. The ground state dipole moments for **16ketPyr** and **18ketPyr** were calculated using DFT methods to be 0.3 D and 16.7 D, compared to TD-DFT calculated excited state dipoles of 0.4 D and 22.0 D, respectively.

Further evidence for the ICT character of the low-energy absorption band of **16ketPyr** and **18ketPyr** was found in solvatochromic and protonation studies. The absorption spectra of **16ketPyr** and **18ketPyr** in non-polar solvents such as toluene are hypsochromically shifted compared to their spectra in more polar solvents, such as chloroform (ESI[†]), where the λ_{max} values for the ICT transitions of **16ketPyr** and **18ketPyr** in toluene are 580 and 570 nm, respectively. In Fig. 2, the effect of a Brønsted acid is apparent; when TFA is added to the same toluene solutions of **16ketPyr** and **18ketPyr**, the broad ICT bands are suppressed because the aniline nitrogens are protonated, and the ICT peaks are regenerated upon the addition of base.

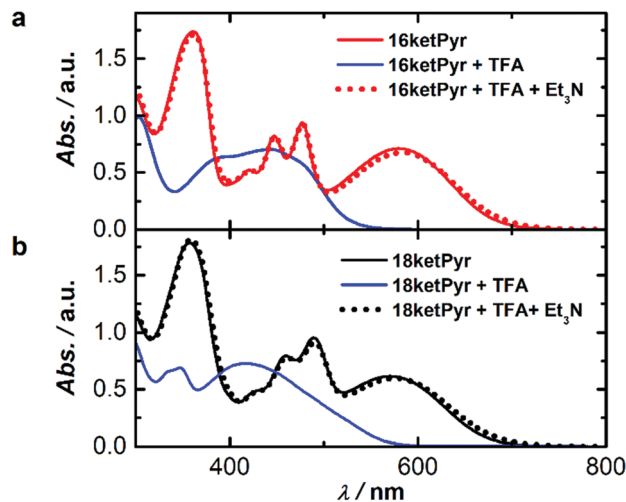


Fig. 2 Absorbance spectra of (a) **16ketPyr** red line and (b) **18ketPyr** black line in toluene solution. Blue lines show resulting spectra after addition of excess TFA, and dotted lines show regenerated spectra upon neutralization with triethylamine.

Effectively, the protonation converts the DAD chromophores into AAA scaffolds, which eliminates the ICT bands. Note the slight red-shift of the Et_3N neutralized spectra compared to the original spectra in toluene; even after addition of a small amount of TFA and Et_3N , the overall polarity of the solution is increased enough to slightly affect the absorbance onset, further supporting the ICT band assignment.

The cyclic and differential pulse voltammograms (DPV) of chromophores **16ketPyr** and **18ketPyr** are shown in the ESI.[†] In terms of the values of the first oxidation and reduction potentials, the two isomers display similar characteristics. Both chromophores oxidize irreversibly at potentials of 0.47 V relative to the Fc/Fc^+ redox couple, and their reductions are also close in energy with compound **18ketPyr** being slightly easier to reduce with a reduction potential of -0.86 V compared to -0.91 V for **16ketPyr**. The largest difference lies in the fact that each electrochemical event is doubled for **16ketPyr**; the C_{2h} symmetric chromophore displays two separate oxidation events, as well as two separate reductions. Similar to our previously reported DAD chromophores, the oxidations were irreversible under cyclic voltammetry experiments using both platinum and carbon working electrodes. The electrochemical reductions of **16ketPyr** and **18ketPyr** were found to be quasi-reversible under the electrochemical conditions used.

Spectroelectrochemical analysis was also carried out on compounds **16ketPyr** and **18ketPyr**, and the spectra are shown in the ESI.[†] In both cases, the ICT band of the chromophores collapses as the acceptor portions of the chromophores are converted into their respective anions, in essence changing the DAD chromophores into DDD systems. However, unlike the compounds reported in our previous work, the original spectra could not be fully regenerated when the applied potential was returned to 0 V, attesting to the quasi-reversibility of the reductions observed in the cyclic voltammograms, suggesting that the anions of **16ketPyr** and **18ketPyr** are not as stable as those of the analogous *ortho*-quinones.^{27,41}

Theoretical calculations

The orbital energy levels of diketones **16ketPyr** and **18ketPyr** calculated using DFT at the B3LYP/6-31+g(d) level as well as the orbital shapes from the ground state calculations are shown in Fig. 3. TD-DFT calculations were found to reflect the experimentally determined absorption spectra for chromophores **16ketPyr** and **18ketPyr** when the polarizable continuum model (PCM) was used to simulate a chloroform solution. Given the C_2 -symmetric DAD design, it was expected that both the HOMO and HOMO-1 energies were nearly degenerate for both chromophores **16ketPyr** and **18ketPyr**, as demonstrated in the ESI.†

The degenerate HOMO and HOMO-1 orbitals of **16ketPyr** and **18ketPyr** are localized predominantly on the ethynyl aniline donor portions of the molecules, but also include MO coefficients on the outer edge of the pyrene ring and the carbonyl oxygen. Interestingly, both the HOMO and HOMO-1 orbitals appear to have nodes on the central naphthalene portion of the pyrene ring. As optical transitions can proceed from either of these orbitals, there are many possible allowed electronic transitions for **16ketPyr** and **18ketPyr**, correlating with their observed multi-peak absorbance spectra shown in Fig. 1. The LUMO orbitals of both chromophores are localized throughout the central pyrene with minor contributions on the ethynyl D-A bridge. TD-DFT calculations predict the lowest energy transition as the one from HOMO to LUMO with a value of 1.57 eV for both isomers, which is in good agreement with the observed optical HOMO-LUMO energy gap of 1.6 eV. The next predicted transition is from the HOMO-1 to the LUMO; this transition is DFT-calculated at 1.7 eV but is only an allowed transition for **18ketPyr**. A summary table, including oscillator strengths, of the TD-DFT computations is in the ESI.† As **18ketPyr** has a higher number of allowed transitions than **16ketPyr**, many of which are close in energy, it is possible that the enhanced molar absorptivity is an additive effect of nearly degenerate transitions that result in stronger absorbance of **18ketPyr** compared to **16ketPyr**.

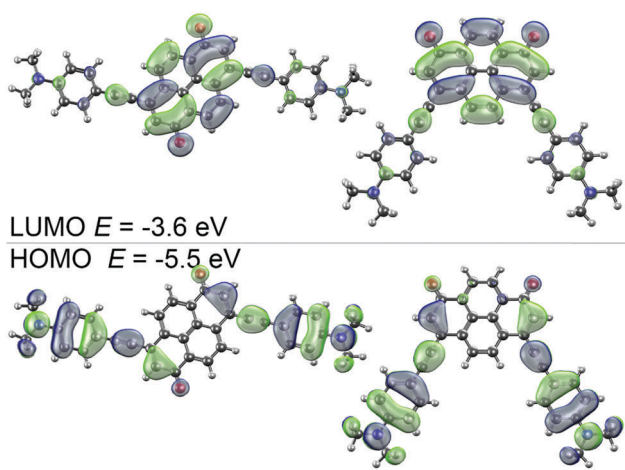


Fig. 3 FMO surfaces calculated for truncated models of **16ketPyr** (left) and **18ketPyr** (right). Surfaces calculated at the B3LYP/6-31+g(d) level of theory and basis set, including the PCM solvent model in chloroform.

Solid state properties

The solid-state behaviour of diketone chromophores **16ketPyr** and **18ketPyr** was investigated, and comparisons are made between the two isomeric compounds in terms of their optical properties in thin films and their thermal properties. Pertinent comparisons are also made between the 1,6- and 1,8-diketones **16ketPyr** and **18ketPyr**, and their *ortho*-diketone structural isomers from previous work.^{27,41}

Diketones **16ketPyr** and **18ketPyr** were subjected to differential scanning calorimetry in order to determine their melting temperatures and to explore the possibility of self-organization into mesophases. Fig. 4 shows the DSC thermograms of **16ketPyr** and **18ketPyr** that were obtained at a heating and cooling rate of 10 °C per minute.

The **18ketPyr** chromophore shows negligible thermal transitions in the temperature range explored save for a broad transition between 0 °C and -15 °C. It is likely that this compound undergoes a slow solidification at these low temperatures, and at higher temperatures exists as a viscous liquid. Heating and cooling a drop-cast sample of **18ketPyr** on the cross-polarized optical microscope (POM) stage revealed no birefringence, hence no long-range ordering for this compound, even at low temperatures. Chromophore **16ketPyr**, on the other hand, showed several transitions in its DSC thermogram. Upon heating diketone **16ketPyr** from room temperature, the compound undergoes an exothermic cold crystallization event, similar to those seen for analogous *ortho*-diketones on their DSC heating curves, with an enthalpy change of 50 J g⁻¹. A melt is then observed at 135 °C, and this melt was also observed for a drop-cast film of chromophore **16ketPyr** under POM. The enthalpy change of the melting transition was determined to be 104 J g⁻¹. As diketone **16ketPyr** is cooled, it undergoes two exothermic phase transitions, which is indicative of the existence of a mesophase between the isotropic liquid and solid phases. The first transition observed upon cooling is at 75 °C, and its associated enthalpy change of 53 J g⁻¹ might be indicative of a transition between an isotropic liquid and a soft-crystalline phase, as the enthalpy change between an isotropic liquid and a liquid

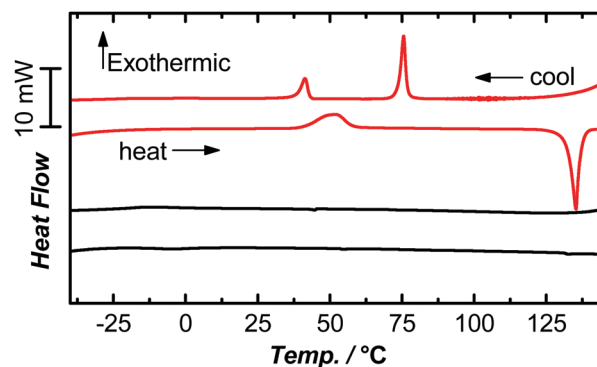


Fig. 4 DSC thermograms of chromophores **16ketPyr** (red) and **18ketPyr** (black). The first cooling and second heating curves are shown. DSC measurements were taken at 10 °C min⁻¹. Exothermic transitions are in the positive direction.

crystal is usually smaller. As **16ketPyr** is cooled from the isotropic liquid to the mesophase on the POM stage, birefringent patterns were observed, as shown in the POM images in Fig. 5. A second exothermic transition takes place at 41 °C, and its associated enthalpy change of 23 J g⁻¹ corresponds to a transition from the mesophase to a crystalline solid.

Spin-cast films of **16ketPyr** and **18ketPyr** were obtained by depositing a saturated chloroform solution of each compound on a 2.5 cm × 2.5 cm glass slide at a spinning rate of 700 rpm for 1.5 minutes. Each slide was examined under POM, as well as UV/Visible absorption spectroscopy. Chromophore **18ketPyr**, which displayed no long-range ordering in the DSC studies, formed a uniform green film on the glass slide that was observed to be amorphous under POM, as was its corresponding drop cast sample. The absorption spectrum of a spin-cast film of **18ketPyr** is plotted in Fig. 6b overlaid with its solution absorption spectrum in chloroform.

For the *ortho*-diketone DAD chromophores in our previous work, there has been a trend in the film absorbances showing that compounds with larger dipole moments show film absorbance spectra that are similar to or even red-shifted compared to their solution absorbance spectra in more polar solvents such as chloroform. Compounds with no overall dipole moment, such as our previous pyrene-tetraketone,²⁷ showed film absorption spectra indicative of a more non-polar solid-state environment, with the λ_{max} of the ICT transition similar to the absorbance in non-polar solvents such as toluene. Note, the correlation between peak positions in the solid-state absorption spectra and the polarity of solvent represents a simplistic view because solid-state solvatochromic features are a combination of a variety of complex interactions, such as molecular aggregation, orientation, dielectric constants, doping and film forming conditions. More detail on the solid-state packing effects on

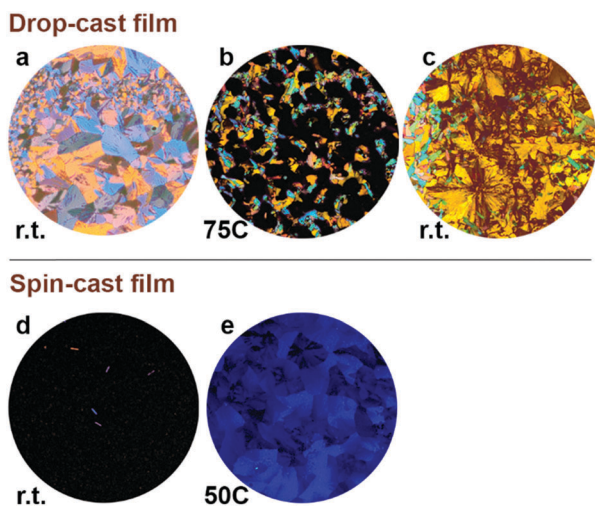


Fig. 5 Polarized optical micrographs (100× magnification) of drop-cast (a–c) and spin-cast (d and e) films of diketone **16ketPyr**. (a) As-cast room temperature image of **16ketPyr**; (b) melted, then cooled to 75 °C image of **16ketPyr**; (c) melted film of **16ketPyr** returned to room temperature; (d) spin-cast film of **16ketPyr**; (e) spin-cast film of **16ketPyr** annealed at 50 °C for 10 minutes.

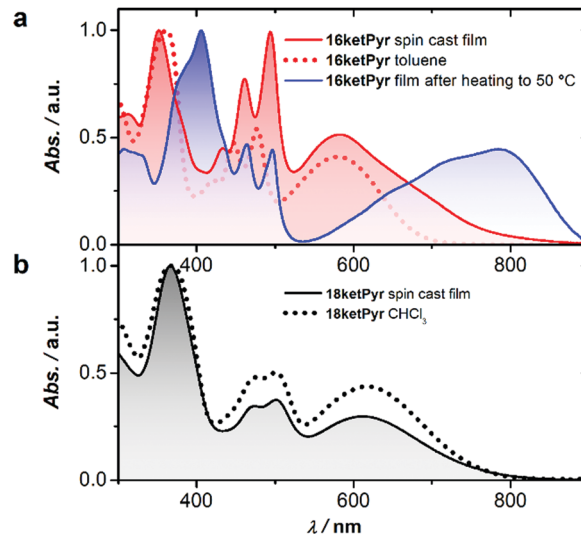


Fig. 6 Normalized absorbance spectra of diketones **16ketPyr** and **18ketPyr**. (a) Compound **16ketPyr** in toluene solution (dotted line), and as a spin-cast film before heating (solid red line) and after heating to 50 °C (solid blue line). (b) Diketone **18ketPyr** in chloroform solution (dashed black line) and spin-cast film (solid black line).

absorption spectra can be found elsewhere.^{51–53} In this limited series of pyrene DAD chromophores, **18ketPyr** has a film absorbance indicative of a more polar solid-state environment; its λ_{max} in the spin-cast film is 613 nm, which is close to that of 617 nm obtained in chloroform.

However, when chromophore **16ketPyr** was spin-cast, as opposed to drop-cast, at room temperature, the film initially formed a uniform but amorphous green film on the glass slide, aside from a few small needle shaped microcrystals, which were observed under POM, shown in Fig. 5d. The absorption spectrum of the amorphous film, shown in Fig. 6a, is similar to the solution absorbance of **16ketPyr** in toluene with a λ_{max} of 581 nm. This is consistent with the overall trend for series of related pyrene DAD chromophores; the near zero dipole moment of **16ketPyr** causes the amorphous solid to behave as if it were in a non-polar medium. However, the onset of absorption of **16ketPyr** in the solid-state is still quite far into the low-energy region of the absorption spectrum at 820 nm, which corresponds to a small decrease in the HOMO–LUMO energy gap of **16ketPyr** compared to the value calculated from the chloroform absorbance spectrum.

As the spin-cast film of **16ketPyr** was heated and maintained at a temperature of 50 °C on the POM stage, birefringent patterns emerged, as shown in Fig. 5e. This observation is consistent with the recrystallization event observed in the DSC trace of **16ketPyr**. The birefringent patterns were retained even after the film of **16ketPyr** was re-cooled to room temperature. The large difference between the POM images of the drop-cast *versus* spin-cast films is due to both the kinetics of film formation and the thicker drop-cast films.

A second absorption spectrum of **16ketPyr** film was recorded after thermal annealing at the cold crystallization temperature from DSC and the film revealed a dramatic change from the original amorphous film. As shown by the POM image of Fig. 5e

and the blue line in Fig. 6a, the λ_{max} of the ICT absorbance band now appears at 789 nm, a shift of just over 200 nm simply due to a phase transition. In this case, the large red-shift is likely caused by the intermolecular interactions between stacked molecules rather than the relative polarity of the medium. With an absorption onset of over 900 nm, chromophore **16ketPyr** shows the most promising solid-state light-harvesting characteristics of the previously reported pyrene quinone chromophores.^{27,41} Furthermore, we are currently investigating whether the ordered mesophase not only enhances the light-harvesting properties of **16ketPyr**, but also allows it to exhibit enhanced charge mobility.

Conclusions

The goal of this report was to create two new pyrene based DAD chromophores with ketone acceptors at the 1,6- and 1,8-positions of pyrene. Though the unsubstituted diketones are produced as a mixture by chromate oxidation of pyrene, separation of the isomers was achieved in the early stages of the synthesis. These new compounds are structural isomers of each other, but are also structural isomers of previously reported *ortho*-diketones. Diketones **16ketPyr** and **18ketPyr**, with C_{2h} and C_{2v} symmetry, respectively, were both found to have reasonable absorption properties in solution, with several optical transitions reaching molar absorptivities of $10^4 \text{ M}^{-1} \text{ cm}^{-1}$ and an onset of the ICT absorbance at 800 nm. This onset of absorbance for **16ketPyr** and **18ketPyr** is even further into the red region of the electromagnetic spectrum than the analogous *ortho*-diketones,^{27,41} meaning that **16ketPyr** and **18ketPyr** have the smallest HOMO–LUMO energy gaps of the five structurally isomeric molecules. Diketones **16ketPyr** and **18ketPyr** also have the lowest LUMO energy levels of the diketone isomers, at -3.9 eV . However, the reductions were found to be only quasi-reversible. In the solid state, only **16ketPyr** self-organized into what is proposed to be a soft-crystalline mesophase. This self-assembly causes intermolecular electronic interactions between the molecules of **16ketPyr** that causes a large red-shift in the UV/Visible absorption of the film compared to even polar solutions, which is a promising materials property.

Conflicts of interest

There are no conflicts to declare.

Acknowledgements

The authors acknowledge NSERC of Canada Discovery Grants program (RGPIN/04444-2014) for financial support, WestGrid/Compute Canada for use of their computing resources to carry out DFT investigations, SNK thanks NSERC-PGS and AITF for scholarship support.

Notes and references

- 1 X. Feng, J.-Y. Hu, C. Redshaw and T. Yamato, *Chem. – Eur. J.*, 2016, **22**, 11898–11916.
- 2 A. Mateo-Alonso, *Chem. Soc. Rev.*, 2014, **43**, 6311–6324.
- 3 T. M. Figueira-Duarte and K. Müllen, *Chem. Rev.*, 2011, **111**, 7260–7314.
- 4 S. Karuppanan and J.-C. Chambron, *Chem. – Asian J.*, 2011, **6**, 964–984.
- 5 J. Duhamel, *Langmuir*, 2012, **28**, 6527–6538.
- 6 F. M. Winnik, *Chem. Rev.*, 1993, **93**, 587–614.
- 7 R. S. Sprick, J.-X. Jiang, B. Bonillo, S. Ren, T. Ratvijitvech, P. Guiglion, M. A. Zwijnenburg, D. J. Adams and A. I. Cooper, *J. Am. Chem. Soc.*, 2015, **137**, 3265–3270.
- 8 M. Yasutake, T. Fujihara, A. Nagasawa, K. Moriya and T. Hirose, *Eur. J. Org. Chem.*, 2008, 4120–4125.
- 9 T. M. Figueira-Duarte and K. Müllen, *Chem. Rev.*, 2011, **111**, 7260–7314.
- 10 P. Somerharju, *Chem. Phys. Lipids*, 2002, **116**, 57–74.
- 11 M. E. Ostergaard and P. J. Hrdlicka, *Chem. Soc. Rev.*, 2011, **40**, 5771–5788.
- 12 A. Hayer, V. de Halleux, A. Köhler, A. El-Garouhy, E. W. Meijer, J. Barberá, J. Tant, J. Levin, M. Lehmann, J. Gierschner, J. Cornil and Y. H. Geerts, *J. Phys. Chem. B*, 2006, **110**, 7653–7659.
- 13 S. Diring, F. Camerel, B. Donnio, T. Dintzer, S. Toffanin, R. Capelli, M. Muccini and R. Ziessel, *J. Am. Chem. Soc.*, 2009, **131**, 18177–18185.
- 14 Y. Sagara and T. Kato, *Angew. Chem., Int. Ed.*, 2008, **47**, 5175–5178.
- 15 V. de Halleux, J. P. Calbert, P. Brocorens, J. Cornil, J. P. Declercq, J. L. Brédas and Y. Geerts, *Adv. Funct. Mater.*, 2004, **14**, 649–659.
- 16 B. R. Kaafarani, L. A. Lucas, B. Wex and G. E. Jabbour, *Tetrahedron Lett.*, 2007, **48**, 5995–5998.
- 17 X. Chen, M. Addicoat, E. Jin, H. Xu, T. Hayashi, F. Xu, N. Huang, S. Irle and D. Jiang, *Sci. Rep.*, 2015, **5**, 14650.
- 18 D. Bessinger, L. Ascherl, F. Auras and T. Bein, *J. Am. Chem. Soc.*, 2017, **139**, 12035–12042.
- 19 S. S. Babu, V. K. Praveen and A. Ajayaghosh, *Chem. Rev.*, 2014, **114**, 1973–2129.
- 20 H. Ju, K. Wang, J. Zhang, H. Geng, Z. Liu, G. Zhang, Y. Zhao and D. Zhang, *Chem. Mater.*, 2017, **29**, 3580–3588.
- 21 J. A. Mikroyannidis, *Synth. Met.*, 2005, **155**, 125–129.
- 22 Y. Niko, H. Moritomo, H. Sugihara, Y. Suzuki, J. Kawamata and G.-I. Konishi, *J. Mater. Chem. B*, 2015, **3**, 184–190.
- 23 J. K. Salunke, P. Sonar, F. L. Wong, V. A. L. Roy, C. S. Lee and P. P. Wadgaonkar, *Phys. Chem. Chem. Phys.*, 2014, **16**, 23320–23328.
- 24 S. Ji, J. Yang, Q. Yang, S. Liu, M. Chen and J. Zhao, *J. Org. Chem.*, 2009, **74**, 4855–4865.
- 25 Y. O. Lee, T. Pradhan, K. Choi, D. H. Choi, J. H. Lee and J. S. Kim, *Tetrahedron*, 2013, **69**, 5908–5912.
- 26 A. Kathiravan, V. Srinivasan, T. Khamrang, M. Velusamy, M. Jaccob, N. Pavithra, S. Anandan and K. Velappan, *Phys. Chem. Chem. Phys.*, 2017, **19**, 3125–3135.

- 27 S. N. Keller, A. D. Bromby and T. C. Sutherland, *Eur. J. Org. Chem.*, 2017, 3980–3985.
- 28 E. Sefer, S. O. Hacıoglu, M. Tonga, L. Toppare, A. Cirpan and S. Koyuncu, *Macromol. Chem. Phys.*, 2015, **216**, 829–836.
- 29 C.-C. Yu, K.-J. Jiang, J.-H. Huang, F. Zhang, X. Bao, F.-W. Wang, L.-M. Yang and Y. Song, *Org. Electron.*, 2013, **14**, 445–450.
- 30 T. Fiebig, W. Kühnle and H. Staerk, *Chem. Phys. Lett.*, 1998, **282**, 7–15.
- 31 E. Pandurski and T. Fiebig, *Chem. Phys. Lett.*, 2002, **357**, 272–278.
- 32 S. Hagopian and L. A. Singer, *J. Am. Chem. Soc.*, 1983, **105**, 6760–6761.
- 33 S. Hagopian and L. A. Singer, *J. Am. Chem. Soc.*, 1985, **107**, 1874–1880.
- 34 A. Wiessner, G. Huettmann, W. Kuehnle and H. Staerk, *J. Phys. Chem.*, 1995, **99**, 14923–14930.
- 35 J. Daub, R. Engl, J. Kurzawa, S. E. Miller, S. Schneider, A. Stockmann and M. R. Wasielewski, *J. Phys. Chem. A*, 2001, **105**, 5655–5665.
- 36 N. Acar, J. Kurzawa, N. Fritz, A. Stockmann, C. Roman, S. Schneider and T. Clark, *J. Phys. Chem. A*, 2003, **107**, 9530–9541.
- 37 E. C. P. Smits, S. G. J. Mathijssen, P. A. van Hal, S. Setayesh, T. C. T. Geuns, K. A. H. A. Mutsaers, E. Cantatore, H. J. Wondergem, O. Werzer, R. Resel, M. Kemerink, S. Kirchmeyer, A. M. Muzafarov, S. A. Ponomarenko, B. de Boer, P. W. M. Blom and D. M. de Leeuw, *Nature*, 2008, **455**, 956–959.
- 38 L. Zang, Y. Che and J. S. Moore, *Acc. Chem. Res.*, 2008, **41**, 1596–1608.
- 39 T. Marszalek, M. Li and W. Pisula, *Chem. Commun.*, 2016, **52**, 10938–10947.
- 40 M. R. Wasielewski, *Acc. Chem. Res.*, 2009, **42**, 1910–1921.
- 41 S. N. Keller, N. L. Veltri and T. C. Sutherland, *Org. Lett.*, 2013, **15**, 4798–4801.
- 42 H. Cho and R. G. Harvey, *J. Chem. Soc., Perkin Trans. 1*, 1976, 836–839, DOI: 10.1039/P19760000836.
- 43 J. Xu, S. Semin, D. Niedzialek, P. H. J. Kouwer, E. Fron, E. Coutino, M. Savoini, Y. Li, J. Hofkens, H. Uji-I, D. Beljonne, T. Rasing and A. E. Rowan, *Adv. Mater.*, 2013, **25**, 2084–2089.
- 44 Y. Duan, C. Ju, G. Yang, E. Fron, E. Coutino-Gonzalez, S. Semin, C. Fan, R. S. Balok, J. Cremers, P. Tinnemans, Y. Feng, Y. Li, J. Hofkens, A. E. Rowan, T. Rasing and J. Xu, *Adv. Funct. Mater.*, 2016, **26**, 8968–8977.
- 45 X. Li, S. Semin, L. A. Estrada, C. Yuan, Y. Duan, J. Cremers, P. Tinnemans, P. Kouwer, A. E. Rowan, T. Rasing and J. Xu, *Chin. Chem. Lett.*, 2017, DOI: 10.1016/j.ccl.2017.11.001.
- 46 A. Lopez-Moreno, D. Clemente-Tejeda, J. Calbo, A. Naeimi, F. A. Bermejo, E. Orti and E. M. Perez, *Chem. Commun.*, 2014, **50**, 9372–9375.
- 47 A. J. Fatiadi, *J. Chromatogr. A*, 1965, **20**, 319–324.
- 48 C. Graebe, *Justus Liebigs Ann. Chem.*, 1871, **158**, 285–299.
- 49 H. Vollmann, H. Becker, M. Corell and H. Streeck, *Justus Liebigs Ann. Chem.*, 1937, **531**, 1–159.
- 50 C. Diner, D. E. Scott, R. R. Tykwinski, M. R. Gray and J. M. Stryker, *J. Org. Chem.*, 2015, **80**, 1719–1726.
- 51 X.-H. Zhou, J. Luo, J. A. Davies, S. Huang and A. K. Y. Jen, *J. Mater. Chem.*, 2012, **22**, 16390–16398.
- 52 J. Wu, W. Wang, C. Gong, Q. Li, Z. Li, G. Deng, X. Zhang, K. Chen, Y. Gong and K. S. Chiang, *J. Mater. Chem. C*, 2017, **5**, 7472–7478.
- 53 J. Wu, H. Xiao, L. Qiu, Z. Zhen, X. Liu and S. Bo, *RSC Adv.*, 2014, **4**, 49737–49744.